Reverberation of flexural waves scattered by a local heterogeneity in a plate

Hossep Achdjian, Emmanuel Moulin, Farouk Benmeddour, Jamal Assaad, Lucie Dupont, Lynda Chehami

JULY 11 2016

Reverberation of flexural waves scattered by a local heterogeneity in a plate

Hossep Achdjian; Emmanuel Moulin; Farouk Benmeddour; Jamal Assaad; Lucie Dupont; Lynda Chehami

J. Acoust. Soc. Am. 140, 157–164 (2016)
https://doi.org/10.1121/1.4954747

Reverberation of flexural waves scattered by a local heterogeneity in a plate

Hossep Achdjian, Emmanuel Moulin,[a] Farouk Benmeddour, Jamal Assaad, Lucie Dupont, and Lynda Chehami

Institut d'Electronique, Microélectronique et Nanotechnologies (IEMN), Unité Mixte de Recherche, CNRS 8520, Université de Valenciennes et du Hainaut-Cambrésis, F-59313 Valenciennes cedex 9, France

(Received 4 January 2016; revised 27 May 2016; accepted 8 June 2016; published online 11 July 2016)

A statistical model is proposed to relate the scattering properties of a local heterogeneity in a plate to the statistical properties of scattered and reverberated flexural waves. The contribution of the heterogeneity is isolated through the computation of differential signals consisting of a subtraction of the signals recorded after and before introduction of the heterogeneity. The theoretical expression of the average reverberation envelope of these differential signals is obtained as a function of the scattering cross-section of the heterogeneity. Successful numerical and experimental validations in various cases of canonical heterogeneities with known scattering cross-sections are shown. These satisfying results offer a way to estimate the scattering cross-section of an unknown scatterer from the reverberated differential signals. © *2016 Acoustical Society of America*.
[http://dx.doi.org/10.1121/1.4954747]

[JFL] Pages: 157–164

I. INTRODUCTION

Wave physics problems in situations where a high number of propagation paths are possible may be judiciously treated as a random process. Such approaches are well known, for example, in multiple scattering[1–4] or reverberation.[5–9] In a closed medium with low attenuation, in particular, multiple reflections at the boundaries create long reverberation tails (also called codas) in the acoustic signals received after emission of an impulse source. These codas correspond to the superposition of numerous wavepackets having travelled the whole medium. Probably the most common application of ensemble averaging of reverberated acoustic signals is in room acoustics. The reverberation time can be easily extracted from envelope averaging or Schroeder's backward integration technique.[10] Then, using either Sabine's or Eyring's law, or some generalized version of them, sound absorption coefficients of walls can be estimated.[11] This well known example constitutes a basic illustration of the fact that extraction of average features on apparently random signals may give access to some useful characteristic properties of the medium.

Recently, the authors have shown how useful information can be extracted on a reverberant plate, by both combining averaged coda properties and direct arrivals of flexural waves.[12–14] Depending on what is known about the plate, it is possible to estimate in this manner either the surface area, the average group velocity or the position of the source. These estimations are based on a statistical time-domain model of the distribution of the reverberated wavepackets.

The work proposed in this paper consists in developing and applying a similar kind of model, in order to relate the scattering properties of a local heterogeneity (or defect) to average features of reverberated signals. The contribution from the defect (scattered waves) is isolated by applying a basic subtraction technique. The signal recorded at each receiver in the reference case [plate without defect, see Fig. 1(a)] is subtracted from the one recorded in the same plate after introduction of the defect [Fig. 1(b)]. The subtraction result will be referred to as the differential signal $\Delta s(t)$. If several source-receiver configurations are considered, then a collection of differential signals with some ensemble statistical properties are obtained. The study of these properties is the object of the work presented here. Though scattering of guided waves by holes or inclusions in unbounded (open) plates has been the subject of several theoretical papers,[15–19] the reverberation of scattered waves in a bounded plate and the relationship with open scattering properties are aspects both theoretically original and experimentally useful for defect characterization.

First, in Sec. II of this paper, the principle and main results of the statistical model of plate reverberation derived in previous works[13,20] will be briefly recalled. Then, following the same kind of derivation, the average envelope of the differential (scattered) signals associated to a localized heterogeneity will be theoretically derived in Sec. III. A fundamental term in the obtained expression is the scattering cross-section of the heterogeneity. Hence in Sec. IV, which is dedicated to numerical validation, two types of canonical heterogeneities are considered, for which values of scattering cross-section are known: a circular, infinitely rigid inclusion and a circular hole. Finally, for more realistic validation, experiments with a circular hole are proposed in Sec. V.

II. REVERBERANT PROPAGATION IN A FINITE PLATE

This section will recall the main results obtained in previous works about reverberation of flexural waves in finite

[a]Electronic mail: emmanuel.moulin@univ-valenciennes.fr

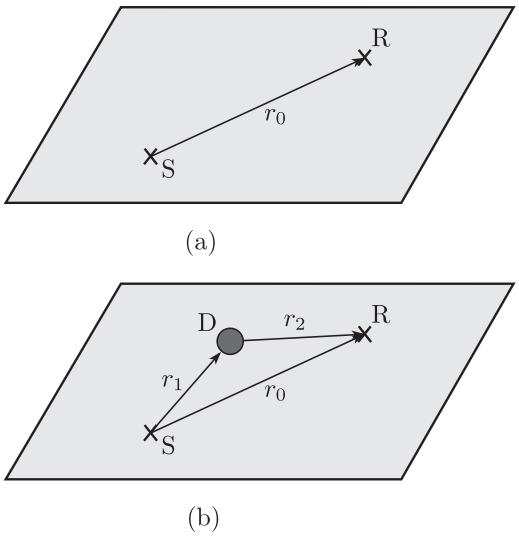

FIG. 1. Schematic description of the case study. (a) Homogeneous reverberant plate with a source (S) and a receiver (R) separated by an arbitrary distance r_0. (b) Same plate, except a local defect (D) is present.

plates.[13,20] Reverberant propagation is described using a statistical model of wavepacket superposition in the time domain, based on the image-source method.[21]

The signal received at a given position after reverberation by the plate boundaries can be expanded as a sum of wavepackets,

$$s_{\text{rev}}(t) = \begin{cases} \sum_{\substack{i=1 \\ r_i \geq r_0}}^{\infty} \kappa_i \, s(r_i, t) & \text{for } t \geq t_0, \\ 0 \quad \text{for } t < t_0, \end{cases} \tag{1}$$

where the subscript "rev" stands for reverberated, κ_i is the number of wavepackets coming from image-sources located at distances between r_i and $r_i + \Delta r_i$ from the receiver, r_0 is the source-receiver distance [see Fig. 1(a)], t_0 the corresponding propagation time, and $s(r_i, t)$ is the signal received after (dispersive) propagation over the distance r_i. In the case of a narrowband excitation $s(r, t)$ can be expressed, for any distance r, as

$$s(r, t) = a(r)\, e^{-\gamma_0 r}\, s_p(r, t), \tag{2}$$

where $a(r)$ is the geometrical spreading term ($1/\sqrt{r}$ in the bidimensional case), γ_0 is the attenuation coefficient (assumed constant in the considered frequency range) and $s_p(r, t)$ represents the propagative component of the wavepacket, which is more conveniently defined by its Fourier transform

$$\tilde{s}_p(r, \omega) = B(\omega)\, \tilde{s}_0(\omega)\, e^{-jk(\omega) r}, \tag{3}$$

with $\tilde{s}_0(\omega)$ the Fourier transform of the excitation signal $s_0(t)$ and $k(\omega)$ the wavenumber. $B(\omega)$ is an excitation amplitude, representing the conversion factor from the source signal to the modal excitation, depending on the generation process (for instance load-induced displacements as in Sec. IV or electromechanical effect as in Sec. V). Besides, it should be noted that γ_0 is a global attenuation constant, accounting for all losses in the propagation and reverberation process (intrinsic material damping, energy losses in the air through leaky waves and reflections at the plate edges).

Statistical treatment consists in considering a given set of source and receiver as one realization of a random process. In that case, κ_i is treated as a random variable, with a mathematical expectation defined as

$$E[\kappa_i] = \lambda(r_i)\, \Delta r_i, \tag{4}$$

where $\lambda(r)$ is the average density of wavepackets propagated over the distance r. In the bidimensional case, $\lambda(r) = \beta_d\, r$ with $\beta_d = 2\pi/\mathcal{S}$ and $\mathcal{S}$ the plate surface area.

Then, it can be shown that the mathematical expectation of the signal envelope is given by

$$E[|S_{\text{rev}}(t)|^2] = A\, e^{-2t/\tau}, \tag{5}$$

where S_{rev} is the complex analytic representation of s_{rev}, $\tau = 1/(\gamma_0 v_{g_0})$ and $v_{g_0} = v_g(\omega_0)$ the group velocity at the central angular frequency ω_0 of the excitation. The amplitude term A is given by

$$A = v_{g_0}\, \beta_d\, D_s, \tag{6}$$

with D_s an energy-related term defined as

$$D_s = \int_0^{+\infty} |B(\omega)\, \tilde{S}_0(\omega)|^2 d\omega. \tag{7}$$

In Sec. III, this kind of statistical model will be extended to the waves scattered by a local heterogeneity (defect) in the plate.

III. REVERBERATION OF SCATTERED WAVES

Consider a source (or indifferently one of its images) S_i located at a distance u_i from the defect (Fig. 2), with an excitation signal $s_0(t)$.

According to Eq. (2), the wavepacket incident on the defect is

$$s(u_i, t) = a(u_i)\, e^{-\gamma_0 u_i}\, s_p(u_i, t). \tag{8}$$

This wavepacket will be scattered by the defect, producing in the far field a diverging wave denoted $s_{\text{sca}|u_i}(r, \theta, t)$

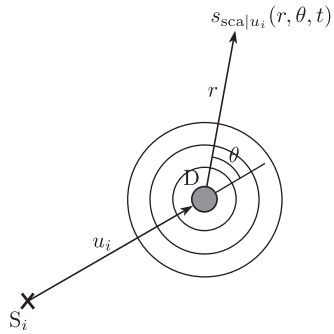

FIG. 2. Scattering of an incident wave from one of the image-sources by the defect.

with an angle-dependent amplitude $f(\theta,\omega)$, and whose Fourier transform can be expressed as

$$\tilde{s}_{\mathrm{sca}|u_i}(r,\theta,\omega)=f(\theta,\omega)\,a(r)\,a(u_i)\,e^{-\gamma_0(r+u_i)}\,\tilde{s}_p(r+u_i,\omega), \tag{9}$$

where the subscript "sca" stands for scattered. This wave scattered by the defect is then reverberated by the plate boundaries and the signal received by the receiver R corresponds to the sum of the wavepackets received by each of its images. Similarly to Eq. (1), this total signal can therefore be expressed as

$$s_{\mathrm{sca,rev}|u_i}(t)=\begin{cases}\displaystyle\sum_{\substack{j=1\\ r_j\geq r_2}}^{\infty}\kappa_j\, s_{\mathrm{sca}|u_i}(r_j,\theta_{ij},t) & \text{for } t\geq r_2/v_{g_0}\,,\\ 0 \quad \text{for } t<r_2/v_{g_0},\end{cases} \tag{10}$$

where the subscript "sca,rev" means "scattered and reverberated," r_2 is the distance from the defect to the receiver [see Fig. 1(b)], r_j is the distance from the defect to the jth image (R_j) of the receiver, θ_{ij} is the value of angle θ (defined in Fig. 2) corresponding to the scattered wavepacket received by R_j, and κ_j has the same definition is in Eq. (1).

This signal $s_{\mathrm{sca,rev}|u_i}(t)$ corresponds to the signal received when the defect scatters the wavepacket coming from a single source (or image-source) S_i located at a distance u_i from the defect. Each image-source will excite the defect at its turn and hence create a similar signal. The total signal at the receiver can then be written as

$$\Delta s(t)=\begin{cases}\displaystyle\sum_{\substack{i=1\\ u_i\geq r_1}}^{\infty}\kappa_i\, s_{\mathrm{sca,rev}|u_i}(t) & \text{for } t\geq r_1/v_{g_0},\\ 0 \quad \text{for } t<r_1/v_{g_0}.\end{cases} \tag{11}$$

For convenience, we will consider in the following that $t\geq(r_1+r_2)/v_{g_0}$. Since the case $t<(r_1+r_2)/v_{g_0}$ corresponds to trivially zero result, it will only be reminded at the end of the derivation.

Then, from Eq. (11), the square of the envelope of $\Delta s(t)$ is

$$|\Delta S(t)|^2=\sum_{i(u_i\geq r_1)}^{+\infty}\kappa_i^2|S_{\mathrm{sca,rev}|u_i}(t)|^2 + \sum_{i}^{+\infty}\sum_{k\neq i}^{+\infty}\kappa_i\kappa_k|S_{\mathrm{sca,rev}|u_i}(t)\,S^{*}_{\mathrm{sca,rev}|u_k}(t)|, \tag{12}$$

where $S_{\mathrm{sca,rev}|u_i}$ is the complex analytic representation of $s_{\mathrm{sca,rev}|u_i}$.

It can be shown that the cross-terms vanish.[20] Therefore,

$$|\Delta S(t)|^2=\sum_{i(u_i\geq r_1)}^{+\infty}\kappa_i^2|S_{\mathrm{sca,rev}|u_i}(t)|^2, \tag{13}$$

and in the same way, using Eq. (10)

$$|S_{\mathrm{sca,rev}|u_i}(t)|^2=\sum_{j(r_j\geq r_2)}^{\infty}\kappa_j^2|S_{\mathrm{sca}|u_i}(r_j,\theta_{ij},t)|^2. \tag{14}$$

Taking the mathematical expectations while assuming independence of the random variables, one obtains

$$E[|\Delta S(t)|^2]=\sum_{i(u_i\geq r_1)}^{+\infty}E[\kappa_i]\,E[|S_{\mathrm{sca,rev}|u_i}(t)|^2] \tag{15}$$

and

$$E[|S_{\mathrm{sca,rev}|u_i}(t)|^2]=\sum_{j(r_j\geq r_2)}^{\infty}E[\kappa_j]\,E[|S_{\mathrm{sca}|u_i}(r_j,\theta_{ij},t)|^2]. \tag{16}$$

Assuming that $f(\theta,\omega)$ is approximately constant in the frequency range (around ω_0), taking the inverse Fourier transform of Eq. (9) and the mathematical expectation of the envelope yields

$$E[|S_{\mathrm{sca}|u_i}(r_j,\theta_{ij},t)|^2]=E[|f(\theta_{ij},\omega_0)|^2]\,a^2(r_j)\,a^2(u_i) \times e^{-2\gamma_0(r_j+u_i)}\,|S_p(r_j+u_i,t)|^2. \tag{17}$$

Assuming uniform probability density for θ_{ij} in the interval $[0,2\pi]$, the mathematical expectation $E[|f(\theta_{ij},\omega_0)|^2]$ can be estimated by an average of $|f(\theta,\omega_0)|^2$ over the interval. Therefore,

$$E\left[|f(\theta_{\mathrm{ij}},\omega_0)|^2\right]\simeq\frac{\sigma_0}{2\pi}, \tag{18}$$

where σ_0 is the scattering cross-section of the defect at frequency ω_0, defined as

$$\sigma_0=\sigma(\omega_0)=\int_0^{2\pi}|f(\theta,\omega_0)|^2d\theta. \tag{19}$$

Introducing Eqs. (17) and (18) into Eq. (16) and replacing sums by integrals yields

$$E\left[|S_{\mathrm{sca,rev}|u_i}(t)|^2\right]=\frac{\sigma_0}{2\pi}\,a^2(u_i)\int_{r_2}^{+\infty}a^2(r)\,\lambda(r) \times e^{-2\gamma_0(r+u_i)}\,|S_p(r+u_i,t)|^2\,dr. \tag{20}$$

Performing a simple change of variables $(v=r+u_i)$ and remarking that $a^2(r)\lambda(r)=\beta_d$, we obtain

$$E\left[|S_{\mathrm{sca,rev}|u_i}(t)|^2\right]=\beta_d\,\frac{\sigma_0}{2\pi}\,a^2(u_i) \times\int_{r_2+u_i}^{+\infty}e^{-2\gamma_0 v}\,|S_p(v,t)|^2\,dv. \tag{21}$$

Since $S_p(r,t)$ is nonzero only for values of r inside a narrow interval around $r_t=v_{g_0}t$, where v_{g_0} is the group

velocity at ω_0, the exponential term varies slightly within that interval and then

$$E\left[|S_{\text{sca,rev}|u_i}(t)|^2\right] \simeq \beta_d \frac{\sigma_0}{2\pi} a^2(u_i)\, e^{-2\gamma_0 r_t} \int_{r_2+u_i}^{+\infty} |S_p(r,t)|^2\, dr. \tag{22}$$

Introducing Eq. (22) into Eq. (15) and replacing the discrete sum by an integral yields

$$E\left[|\Delta S(t)|^2\right] = \beta_d^2 \frac{\sigma_0}{2\pi}\, e^{-2\gamma_0 r_t} \int_{r_1}^{+\infty} \int_{r_2+u}^{+\infty} |S_p(r,t)|^2 dr\, du. \tag{23}$$

Considering once more the properties of the wavepacket corresponding to $S_p(r,t)$, the following approximation can reasonably be made:

$$\int_{r_2+u}^{+\infty} |S_p(r,t)|^2 dr \simeq \begin{cases} \displaystyle\int_0^{+\infty} |S_p(r,t)|^2 dr & \text{for } r_2+u \le r_t, \\ 0 \quad \text{for } r_2+u > r_t. \end{cases} \tag{24}$$

Then Eq. (23) yields

$$E\left[|\Delta S(t)|^2\right] = \beta_d^2 \frac{\sigma_0}{2\pi}\, e^{-2\gamma_0 r_t}\, (r_t - r_2 - r_1) \times \int_0^{+\infty} |S_p(r,t)|^2 dr. \tag{25}$$

As shown in previous works,[20]

$$\int_0^{+\infty} |S_p(r,t)|^2 dr = \int_0^{+\infty} v_g(\omega) |B(\omega)\, \tilde{S}_0(\omega)|^2 d\omega \simeq v_{g_0} D_s, \tag{26}$$

with D_s as defined in Eq. (7).

Then, recalling that $r_t = v_{g_0} t$ and defining $\tau = 1/(\gamma_0 v_{g_0})$, Eq. (25) yields

$$E\left[|\Delta S(t)|^2\right] \simeq \frac{\sigma_0}{\mathcal{S}}\, (v_{g_0} t - r_1 - r_2)\, A\, e^{-2t/\tau}, \tag{27}$$

with $A = 2\pi v_{g_0} D_s/\mathcal{S}$ as defined in Eq. (6).

The presence of both distances r_1 and r_2 in Eq. (27) needs to be briefly commented here. For convenience, they have been implicitly considered as invariants of the random process when taking the mathematical expectations. In a realistic situation, though, averaging would be performed over a set of distributed receivers (and possibly sources), for a fixed scatterer position. In that case, $r_1 + r_2$ would obviously vary. The error introduced by the invariant assumption is minor, especially for large times (when $v_{g_0} t \gg r_1 + r_2$). However, a better approximation for short times can be obtained in replacing $r_1 + r_2$ with an average distance r_a. In cases where the squared-envelope averaging is performed over a set of receivers and with a unique source position, r_a may be defined as $r_1 + r_{2a}$, where r_{2a} is the average distance between the defect and the receivers. More elegantly, an approximate value independent from the particular source and receiver positions may be obtained by defining r_a as

$$r_a = \frac{2}{\mathcal{S}} \int\int_{\mathcal{S}} \sqrt{(x-x_d)^2 + (y-y_d)^2}\, dx\, dy, \tag{28}$$

which corresponds to two times the average distance between the defect position (x_d, y_d) and any point on the plate.

Then, the final theoretical expression of the average squared envelope of reverberated scattered waves is

$$E\left[|\Delta S(t)|^2\right] \simeq \begin{cases} \dfrac{\sigma_0}{\mathcal{S}}\, (v_{g_0} t - r_a)\, A\, e^{-2t/\tau} & \text{for } t \ge r_a/v_{g_0}, \\ 0 \quad \text{for } t < r_a/v_{g_0}. \end{cases} \tag{29}$$

Numerical and experimental validations of this expression will be proposed in Secs. IV and V, respectively. In all presented cases, the range of frequency-plate thickness product is sufficiently low so that a surface excitation will not significantly generate any guided mode other than the flexural one (or A_0 mode). Therefore the model assumption of a single-mode propagation will apply.

IV. NUMERICAL VALIDATION

In this section, the open-source finite element code Elmer[22] is used to simulate the propagation of flexural waves. This code includes a Reissner-Mindlin plate model, which will be perfectly convenient for the range of frequency-plate thickness product considered in this work. In all simulations, the excitation is a time-dependent normal point load $s_0(t)$ applied at the plate surface. From the far-field expression of the Green's function for flexural waves, the excitation amplitude $B(\omega)$ in Eq. (3) can be expressed in this case by

$$B(\omega) = \frac{j-1}{8\, k(\omega)^2\, D\, \sqrt{\pi k(\omega)}}, \tag{30}$$

with $D = Eh^3/[12(1-\nu^2)]$ the bending stiffness, where E, ν, ρ and h are the Young's modulus, the Poisson's ratio, the density and the plate thickness, respectively.

Introducing this expression of $B(\omega)$ into Eq. (7) and assuming a narrowband load excitation $s_0(t)$ of central frequency ω_0 yields

$$D_s \simeq \frac{1}{16\, \pi\, k_0^5\, D^2} \int_0^{+\infty} s_0^2(t)\, dt, \tag{31}$$

where $k_0 = k(\omega_0)$.

The Kirchhoff-Love plate theory allows to approximate the wavenumber and group velocity of flexural waves by $k_0 \simeq \sqrt{\omega_0 \sqrt{\rho h/D}}$ and $v_{g_0} \simeq 2\omega_0/k_0$, respectively. Therefore, from Eqs. (6) and (31), the amplitude of the average of the squared envelope of the reverberated signal can be estimated as

$$A \simeq \frac{1}{4\,\mathcal{S}\,\omega_0^2\,\sqrt{D}\,(\rho h)^{3/2}} \int_0^{+\infty} s_0^2(t)\,dt. \tag{32}$$

Since Eq. (29) depends on the plate surface area $\mathcal{S}$, two plates of different sizes are considered in the simulations:

• Plate 1: 1.5 m × 1 m ($\mathcal{S} = 1.5$ m^2), rectangular, 3 mm thickness, aluminum.

• Plate 2: 0.5 m × 0.3 m ($\mathcal{S} = 0.15$ m^2), rectangular, 3 mm thickness, aluminum.

A defect (scatterer) is modelized by a local modification of the plate properties. For validation purpose, it is necessary to select a canonical type of scatterer for which theoretical estimation of the scattering cross-section σ_0 is available. Here, the two limit cases of a cylindrical inclusion have been considered: an infinitely rigid inclusion (clamped condition on a cylindrical area spanning the whole plate thickness) and a cylindrical through-hole. In both cases, σ_0 has been estimated from the work of Vemula and Norris[16] on the scattering of flexural plate waves. The numerical reverberated scattered waves are obtained from the subtraction of the results of finite element simulations of, first, the plate with the scatterer and, second, the same plate without scatterer (reference state).

The results presented on Fig. 3 concern plate 1. The normal load signal s_0 is a Hanning-windowed sinusoid waveform of frequency $f_0 = \omega_0/2\pi = 10$ kHz and a number of cycles $N_c = 10$. The first step consists in verifying the consistency of the finite element simulation with Eqs. (5) and (32). The numerical averaged envelopes are obtained from the time-dependent normal displacements extracted at 15 randomly distributed positions over the surface of the plate simulated without defect. First, the squared envelopes of these 15 signals are computed from the modulus of their complex analytical representations (numerical Hilbert transform). Then the average of these 15 squared envelopes is computed. Finally, in order to show a result homogeneous to displacement signals, the square root of this average is taken [thin curve in Fig. 3(a)]. The theoretical curve (bold line) is obtained from the square root of Eq. (5). As already observed in previous works,[13,20] a very satisfying agreement is obtained between both curves.

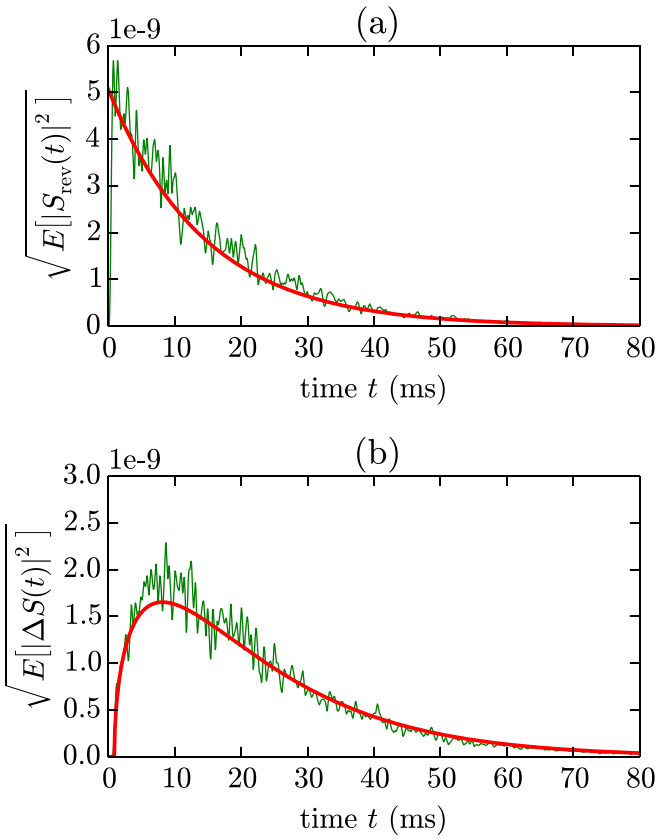

FIG. 3. (Color online) Comparison between theory (bold line) and numerical results (thin line) for plate 1, with $f_0 = 10$ kHz and $N_c = 10$ cycles. (a) Average envelope of reverberated signals, plate without defect. (b) Average envelope of reverberated scattered waves, defect is a rigid inclusion of radius 5 mm ($\sigma_0 = 6.2$ cm).

Now the reverberated scattered waves will be considered. Differential signals are extracted from the subtraction of the signals obtained at the same 15 positions in both the plate with a defect and the reference state. In the first example the defect is an infinitely rigid inclusion of 5 mm radius, centered at position ($x_d = 0.8$ m, $y_d = 0.6$ m) (origin taken at the bottom left corner of the plate). The corresponding scattering cross-section is $\sigma_0 = 6.2$ cm at $f_0 = 10$ kHz. The average envelope of these reverberated scattered signals $\Delta s(t)$ is computed following the same process as described above. The result of this numerical estimation is presented as the thin curve on Fig. 3(b). The increasing evolution for early times is typical of cumulative effects associated to the scattering by the defect of multiply reflected waves at the plate boundaries. Then at later times (corresponding to longer propagation distances and a higher number of reflections), the exponential decrease caused by attenuation eventually becomes the dominating effect. This evolution is well predicted by the theoretical curve (bold line) corresponding to the square root of Eq. (29). The average distance r_a has been determined from Eq. (28) which, in the case of a rectangular plate of sides a and b, can be explicitly calculated as

$$r_a = \frac{2}{ab}[F(x_d, y_d) + F(a - x_d, y_d) + F(x_d, b - y_d) + F(a - x_d, b - y_d)], \tag{33}$$

with

$$F(x,y) = \frac{xy}{3}\sqrt{x^2+y^2} + \frac{y^3}{6}\ln\left(\frac{\sqrt{x^2+y^2}+x}{y}\right) + \frac{x^3}{6}\ln\left(\frac{\sqrt{x^2+y^2}+y}{x}\right). \tag{34}$$

Other results, for the same plate and the same scatterer but at higher frequencies, are presented on Fig. 4. In order to show a set of curves dependent only on the plate and defect properties, and independent from the source amplitude, it is more judicious to normalize with respect to the amplitude term A. Therefore, we represent in the following figures the square root of the averaged squared envelopes of the 15 numerical $\Delta s(t)$ signals, divided by $\sqrt{A}$ (thin curve). In bold

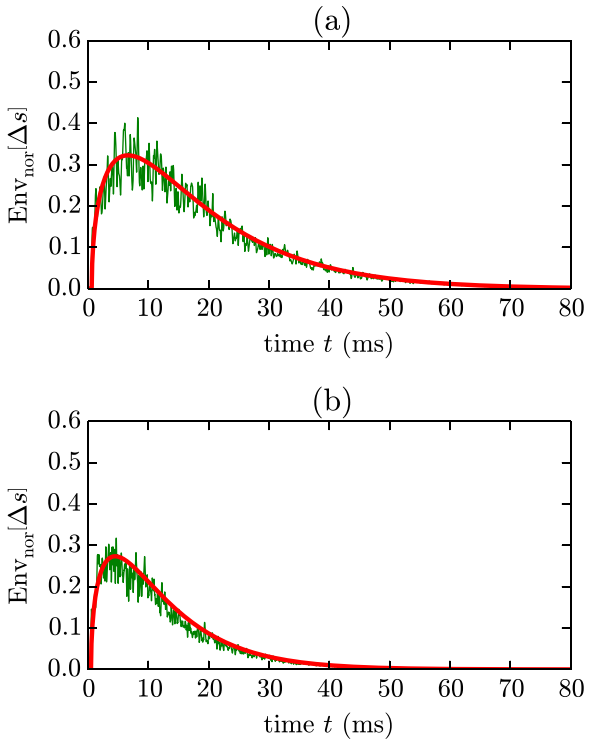

FIG. 4. (Color online) Comparison between theory (bold line) and numerical results (thin line) for plate 1: normalized average envelopes of reverberated scattered waves, defect is a rigid inclusion of radius 5 mm. (a) $f_0 = 20$ kHz ($\sigma_0 = 5.1$ cm), $N_c = 10$ cycles. (b) $f_0 = 30$ kHz ($\sigma_0 = 4.6$ cm), $N_c = 10$ cycles.

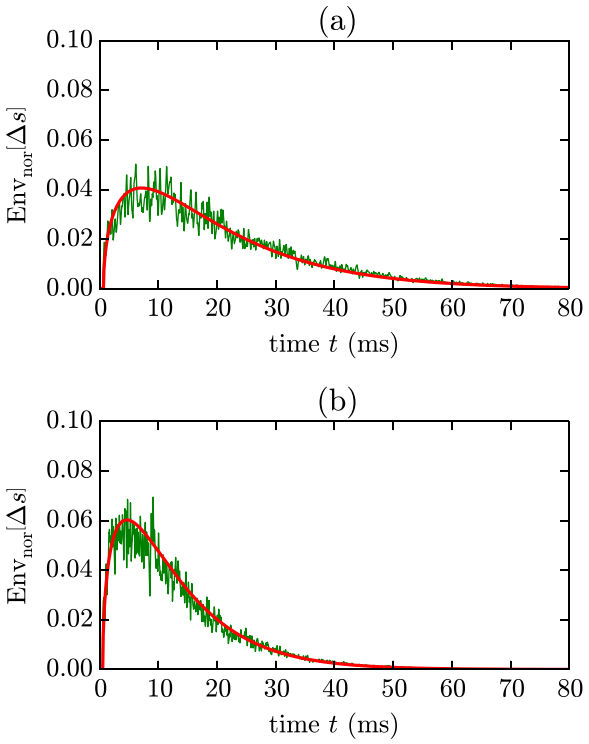

FIG. 5. (Color online) Comparison between theory (bold line) and numerical results (thin line) for plate 1: normalized average envelopes of reverberated scattered waves, defect is a hole of radius 5 mm. (a) $f_0 = 20$ kHz ($\sigma_0 = 0.74$ mm), $N_c = 10$ cycles. (b) $f_0 = 30$ kHz ($\sigma_0 = 2.2$ mm), $N_c = 10$ cycles.

curve, we have also represented for comparison the following theoretical expression naturally derived from Eq. (29): $\mathrm{Env}_{\mathrm{nor}}[\Delta s(t)] = \sqrt{\sigma_0 (v_{g0}\, t - r_a)/\mathcal{S}} e^{-t/\tau}$. For simplicity, we will refer to these quantities as normalized average envelopes. Figure 4(a) corresponds to an excitation frequency $f_0 = 20$ kHz, for which $\sigma_0 = 5.1$ cm. Figure 4(b) corresponds to $f_0 = 30$ kHz and $\sigma_0 = 4.6$ cm. In both cases, the theoretical curve satisfyingly matches the numerical one.

In the following examples, the scatterer will be a through hole of radius 5 mm located at the same position as in the previous case. Since the scattering cross-section is much lower for a hole than for a rigid inclusion of the same diameter, these results will extend the validation range of Eq. (29). Thus, normalized average envelopes are represented in Figs. 5(a) and 5(b) for excitation frequencies 20 kHz ($\sigma_0 = 0.74$ mm) and 30 kHz ($\sigma_0 = 2.2$ mm), respectively, and for the same simulated plate 1. Here again, a satisfying comparison is observed.

Results are less satisfying when considering a smaller plate. Indeed, as shown in Fig. 6(a), it appears that for a frequency of 20 kHz in plate 2 (same hole, centered at $x_d = 0.2$ m, $y_d = 0.1$ m), the average envelope is poorly estimated by the theory. A simple explication of this fact is that the plate boundaries can no longer be considered as in the far field of the scatterer. With a wavelength around 4 cm at 20 kHz, the hole is necessarily within a distance shorter than three to four wavelengths from at least one of the boundaries. Therefore, possible interactions of evanescent waves created around the scatterer and near the boundaries may occur. Since they are not taken into account in the theory (relying on far-field scattering properties only), such evanescent waves would obviously invalidate the predictions. This is a limitation of the current model.

When the excitation frequency is increased, the far field assumption eventually becomes valid again. Hence, a satisfying agreement is shown on Fig. 6(b) for $f_0 = 50$ kHz, at which the minimum hole-boundary distance is more than six wavelengths.

As shown in Sec. V, similar results are obtained experimentally.

V. EXPERIMENTAL RESULTS

Experiments have been carried out on an aluminum plate of lateral dimensions 0.5 m × 0.3 m and 3 mm thickness (same dimensions as plate 2 in the numerical simulations presented in Sec. IV). The plate has been equipped with a set of nine piezoelectric (PZT) patches arbitrarily distributed on its surface. One of them is used as the acoustic source and is fed with an electrical signal $s_0(t)$ provided by a function generator. The other PZT patches are connected to an eight-channel data acquisition board and are used as receivers.

In all the presented cases, the excitation signal s_0 is a Hanning-windowed sinusoid waveform of frequency f_0 and with a duration of N_c cycles. First, the eight received signals have been simultaneously recorded in the defect-less plate. Then a 5 mm-radius through-hole has been drilled in the plate, at position ($x_d = 0.2$ m, $y_d = 0.1$ m) and a second set

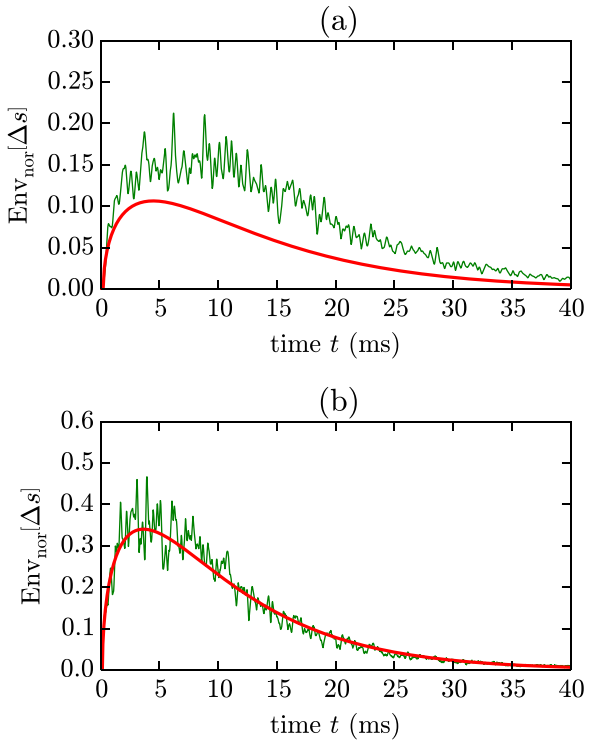

FIG. 6. (Color online) Comparison between theory (bold line) and numerical results (thin line) for plate 2: normalized average envelopes of reverberated scattered waves, defect is a hole of radius 5 mm. (a) $f_0 = 20$ kHz ($\sigma_0 = 0.74$ mm), $N_c = 10$ cycles. (b) $f_0 = 50$ kHz ($\sigma_0 = 5.8$ mm), $N_c = 20$ cycles.

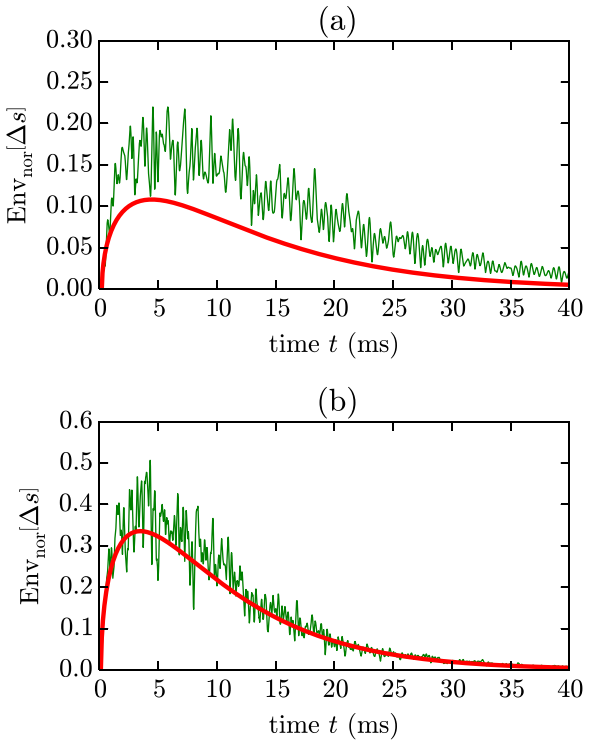

FIG. 7. (Color online) Comparison between theory (bold line) and experimental results (thin line) for plate of dimensions 0.5 m × 0.3 m, 3 mm thickness: normalized average envelopes of reverberated scattered waves, defect is a hole of radius 5 mm. (a) $f_0 = 20$ kHz ($\sigma_0 = 0.74$ mm), $N_c = 10$ cycles. (b) $f_0 = 50$ kHz ($\sigma_0 = 5.8$ mm), $N_c = 20$ cycles.

of acquisitions has been recorded. After subtraction of the records made after and before the hole drilling, respectively, the same process as with the numerical subtraction signals has been applied: computation of the squared envelopes, average, division by the amplitude term A (normalization) and square root of the result. It should be noted, however, that since the excitation is provided by a PZT patch bonded on the plate surface, direct estimation of A [as is the case in the numerical case from Eq. (32)] would be really difficult. Indeed, this would require a perfect knowledge of the electromechanical patch properties and the bonding characteristics, which is hardly realistic. Instead, as explained in previous works,[13] it is possible to estimate A from a mere curve fitting applied to the averaged squared envelope of the reverberated signals in the defect-less plate.

The obtained experimental results are shown in thin curves in Figs. 7 and 8, for different frequencies ranging from 20 to 80 kHz. The theoretical envelopes obtained from Eq. (29) have also been represented in each case for comparison (bold curves).

For excitation frequencies of 20 and 50 kHz [Figs. 7(a) and 7(b), respectively], the obtained results are very similar to the numerical ones (presented in Fig. 6). The main noticeable difference is the higher dispersion (or oscillations) of the experimental envelopes around their average values. This is merely due to the fact that the numerical envelopes are obtained from an average over 15 sensor positions, whereas the experimental ones are obtained from 8 sensors only. This direct comparison between Figs. 7 and 6 tends to

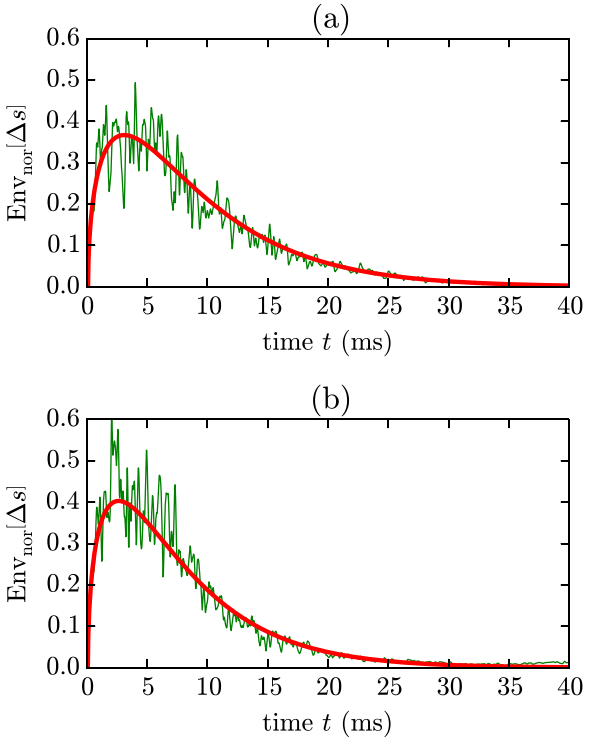

FIG. 8. (Color online) Comparison between theory (bold line) and experimental results (thin line) for plate of dimensions 0.5 m × 0.3 m, 3 mm thickness: normalized average envelopes of reverberated scattered waves, defect is a hole of radius 5 mm. (a) $f_0 = 60$ kHz ($\sigma_0 = 7.1$ mm), $N_c = 25$ cycles. (b) $f_0 = 80$ kHz ($\sigma_0 = 8.8$ mm), $N_c = 30$ cycles.

prove in particular, that the mismatch observed for longer wavelengths (example here at 20 kHz) is neither caused by some numerical bias nor some experimental uncertainty.

Finally, experimental results at higher frequencies are presented on Fig. 8. A very good agreement with the theoretical envelopes is observed. These results confirm the validity of the theory, provided the wavelength is small compared to the lateral plate dimensions.

VI. CONCLUSION

The work presented here establishes a direct relationship between the scattering properties of a local heterogeneity in a plate and the statistical features of differential signals obtained from subtraction of waveforms recorded after and before introduction of the heterogeneity.

A statistical model has been developed, based on average distribution of scattered and reverberated wavepackets. This model is valid in the case of single-mode propagation (here flexural waves) and provided the defect is at a distance of more than a few wavelengths from all plate boundaries (far-field assumption). In those conditions, the mathematical expectation of the squared envelope of the differential signals has been explicitly related to both the plate and scatterer characteristics. In particular, the amplitude of the theoretical envelope is shown to be proportional to the square root of the scattering cross-section of the heterogeneity.

Both numerical and experimental validations of the theory have been demonstrated. The average of the envelopes of differential signals, collected on a set of receivers distributed over the plate surface, compares satisfyingly to the theoretical expectation.

These results provide a way of directly estimating the scattering cross-section of an unknown defect, without the impractical requirement of isolating the first wavepackets from the reflected ones. Therefore, this could serve as a reference technique in situations where a quantitative characterization of a defect in a bounded medium is needed.

ACKNOWLEDGMENT

This work has been partially supported by the French National Research Agency (ANR): ANR2011 BS0903901, PASNI project.

[1]P. C. Waterman and R. Truell, "Multiple scattering of waves," J. Mathematical Phys. **2**, 512–537 (1961).
[2]M. van der Baan, "Acoustic wave propagation in one-dimensional random media: the wave localization approach," Geophys. J. Internat. **145**, 631–646 (2001).
[3]E. Larose, P. Roux, M. Campillo, and A. Derode, "Fluctuations of correlations and Green's function reconstruction: Role of scattering," J. Appl. Phys. **103**, 114907 (2008).
[4]A. Aubry and A. Derode, "Detection and imaging in a random medium: A matrix method to overcome multiple scattering and aberration," J. Appl. Phys. **106**, 044903 (2009).
[5]J.-L. Davy, "The ensemble variance of random noise in a reverberation room," J. Sound Vib. **107**, 361–373 (1986).
[6]T. W. Bartel and S. L. Yaniv, "Curvature of sound decays in partially reverberant rooms," J. Acoust. Soc. Am. **72**, 1838–1844 (1982).
[7]J. Burkhardt and R. L. Weaver, "The effect of decay rate variability on statistical response predictions in acoustic systems," J. Sound Vib. **196**, 147–164 (1996).
[8]C. Draeger, J.-C. Aime, and M. Fink, "One-channel time-reversal in chaotic cavities: Experimental results," J. Acoust. Soc. Am. **105**, 618–625 (1999).
[9]S. Catheline, T. Gallot, P. Roux, G. Ribay, and J. de. Rosny, "Coherent backscattering enhancement in cavities: The simple-shape cavity revisited," Wave Motion **48**, 214–222 (2011).
[10]W. T. Chu, "Comparison of reverberation measurements using Schroeder's impulse method and decay-curve averaging method," J. Acoust. Soc. Am. **63**, 1444–1450 (1978).
[11]J. Ducourneau and V. Planeau, "The average absorption coefficient for enclosed spaces with non uniformly distributed absorption," Appl. Acoust. **64**, 845–862 (2003).
[12]E. Moulin, H. Achdjian, J. Assaad, F. Benmeddour, K. Hourany, and Y. Zaatar, "Statistical model of the impulse response of a reverberant plate: Application to parameter estimation and correlation analysis," in *Proceedings of the 11th Congress Franais d'Acoustique Joint With 2012 Annual IOA Meeting*, Nantes, France (2012), pp. 685–691.
[13]H. Achdjian, E. Moulin, F. Benmeddour, J. Assaad, and L. Chehami, "Source localisation in a reverberant plate using average coda properties and early signal strength," Acta Acust. Acust. **100**, 834–841 (2014).
[14]H. Achdjian, E. Moulin, F. Benmeddour, and J. Assaad, "Estimation of the area of a reverberant plate using average reverberation properties," Phys. Procedia **70**, 139–142 (2015).
[15]Y. H. Pao and C. C. Mow, *Diffraction of Elastic Waves and Dynamics Stress Concentration* (Crane-Russak, New York, 1972).
[16]C. Vemula and A. N. Norris, "Flexural wave propagation and scattering on thin plates using Mindlin theory," Wave Motion **26**, 1–12 (1997).
[17]J. C. P. McKeon and M. K. Hinders, "Lamb wave scattering from a through hole," J. Sound Vib. **224**, 843–862 (1999).
[18]T. Grahn, "Lamb wave scattering from a circular partly through-thickness hole in a plate," Wave Motion **37**, 63–80 (2003).
[19]W. M. Lee and J. T. Chen, "Scattering of flexural wave in a thin plate with multiple circular inclusions by using the null-field integral equation approach," J. Sound Vib. **329**, 1042–1061 (2010).
[20]E. Moulin, H. Achdjian, J. Assaad, N. Abou Leyla, K. Hourany, and Y. Zaatar, "Extraction of the statistical properties of the point source response of a reverberant plate and application to parameter estimation," J. Acoust. Soc. Am. **132**, 2165–2168 (2012).
[21]J. Cuenca, F. Gautier, and L. Simon, "Harmonic Green's functions for flexural waves in semi-infinite plates with arbitrary boundary conditions and high-frequency approximation for convex polygonal plates," J. Sound Vib. **331**, 1426–1440 (2012).
[22]Elmer is an open source multiphysical finite element simulation software mainly developed by CSC - IT Center for Science (CSC). Elmer development was started in 1995 in collaboration with Finnish Universities, research institutes, and industry. It includes physical models of fluid dynamics, structural mechanics, electromagnetics, heat transfer and acoustics. See https://www.csc.fi/web/elmer for more details.